Direct visualisation, by aberration-corrected electron microscopy, of the crystallisation of bimetallic nanoparticle catalysts

Edmund P. W. Ward,*[a] Ilke Arslan,[a] Paul A. Midgley,*[a] Andrew Bleloch[b] and John Meurig Thomas*[ac]

Received (in Cambridge, UK) 3rd August 2005, Accepted 27th September 2005
First published as an Advance Article on the web 20th October 2005
DOI: 10.1039/b511004a

Using a scanning transmission electron microscope, corrected for aberration, ultra-high resolution images of the internal structure of nanoparticle clusters, as well as the number of atoms present per cluster, may be directly determined: it is shown that individual bimetallic clusters of $Ru_{10}Pt_2$ have a "molecular" structure and that when they coalesce into larger entities containing *ca.* 200 atoms they adopt the regular crystalline, and facetted, state of a bulk metal.

Bimetallic catalysts consisting of between six and sixteen atoms, supported on silica surfaces, are extremely active and selective in the hydrogenation of a number of key organic compounds.[1,2] Typical examples are $Ru_{12}Cu_4$, $Ru_{12}Ag_4$, Ru_5Pt and $Ru_{10}Pt_2$,[3] all of which may be readily prepared[4,5] with well-defined stoichiometry from their parent mixed-metal carbonylates. Notwithstanding the remarkable performance that these nanoparticle catalysts exhibit, much remains to be understood concerning their structure and electronic properties. In this communication, we present the results of a high-resolution (real-space) scanning transmission electron microscopy (STEM)[6] study, using the SuperSTEM facility at CCLRC, Daresbury,[7] to investigate directly the internal structure of bimetallic nanoparticles of $Ru_{10}Pt_2$†, which are powerful catalysts for the conversion of muconic acid to adipic acid.[8]

The SuperSTEM is a dedicated, aberration-corrected STEM, consisting of a Vacuum Generators (VG) HB501 FEG (field-emission gun) instrument corrected to third order using a combination of dipole, quadrupole and octupole elements, and, under ideal operating conditions, has sub-Ångstrom imaging capability. Collection of the incoherent, high-angle annular dark field (HAADF) signal, as shown in Fig. 1, gives excellent contrast when imaging the nanoparticles supported on mesoporous silica. HAADF-STEM, often described as Z-contrast (atomic number) imaging since the measured intensity is approximately proportional to the square of the atomic number,[9] is a powerful high-resolution technique that generates readily interpretable images of nanoscale structures. The technique is relatively insensitive to sample thickness and defocus, and a particular benefit to the present work is that the technique permits the calculation (see below) of the number of atoms present within a particular nanoparticle. In this manner, one is able to probe changes in structure as a function of size.

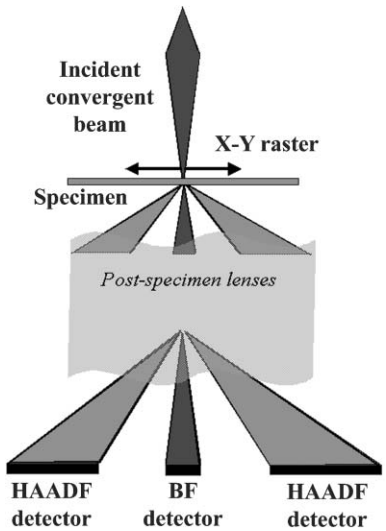

Fig. 1 Schematic of a scanning transmission electron microscope (STEM), showing the position of bright-field (BF) and high-angle annular dark-field (HAADF) detectors. As the probe is scanned across the specimen, the high collection angle (greater than 70 mrad) of the HAADF detector records a signal dominated by incoherent, thermal diffuse scattering. This intensity is insensitive to sample thickness, probe defocus, and the coherent Bragg (diffraction) contrast characteristic of conventional transmission electron microscopy.

Although, in general, the bimetallic nanoparticles described by us in previous studies are monodisperse[1,2,4,5] and unusually resistant to sintering, in certain circumstances the act of loading these nanoparticles onto the silica and subsequent mounting (for microscopy) on 'holey' carbon films, favours the coalescence of between 6 and 12 individual clusters (in the case of $Ru_{10}Pt_2$). Such a distribution of sizes is seen in Fig. 2; and Table 1 presents representative data pertaining to the mean number of metal atoms per particle. Histograms (not shown) of nanoparticle size were calculated using software scripts written in IDL.[10]‡ It was found that the histograms recorded before and after use of the nanoparticles as catalysts were essentially indistinguishable. In order to estimate particle volume from projected area, particles were assumed to be spherical, and calculation of the number of atoms within a cluster was accomplished using the bulk density of the majority constituent, such that the volume occupied by a single Ru atom was assumed to be 0.0136 nm^3.

Figs. 3 and 4 show representative examples of, respectively, a loose agglomerate of individual nanoparticles and a coalesced,

[a]*Department of Materials Science and Metallurgy, University of Cambridge, Pembroke Street, Cambridge, UK CB2 3QZ. E-mail: epww2@cam.ac.uk (EPWW); pam33@cam.ac.uk (PAM); jmt2@cam.ac.uk (JMT)*
[b]*UK SuperSTEM, Daresbury Laboratory, Daresbury, Cheshire, UK WA4 4AD*
[c]*Davy Faraday Research Laboratory, The Royal Institution of Great Britain, 21 Albemarle Street, London, UK W1X 4BS*

Table 1 Properties of the nanoparticle size distribution before and after catalysis. Errors in the mean number of atoms per particle are quoted to within one standard deviation of a fitted Poisson curve

Sample	Number of particles analysed	Mean volume/nm^3	Mean number of atoms per particle
$Ru_{10}Pt_2$ before catalysis	212	1.88	140 $\pm$ 12
$Ru_{10}Pt_2$ after catalysis	364	1.66	120 $\pm$ 11

crystalline (larger) nanoparticle, in which both the lattice fringes and the facetting of the periphery are clearly apparent.

Comparatively little information is available concerning the internal structure of supported bimetallic nanoparticles (or monometallic ones of comparable size). Extended X-ray absorption fine structure (EXAFS) is a useful probe to address such questions, and an earlier study[8] yielded a model in which the bond lengths of both Ru and Pt to the oxygen of the support were deduced (Ru–O = 1.95, Pt–O = 2.08 Å). Such work reinforces the view that, with small nanoparticle bimetallic clusters, it is appropriate to regard the bimetallic entity as a molecule bound by ionic-covalent linkage to the silica support.

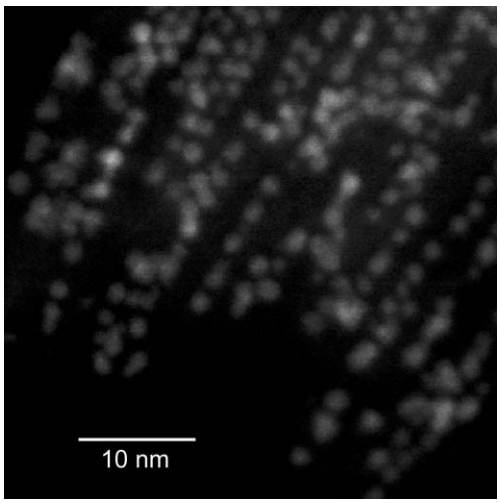

Fig. 2 STEM HAADF image of $Ru_{10}Pt_2$ supported on mesoporous silica (note alignment of clusters along the pores). Note also the range of nanoparticle sizes.

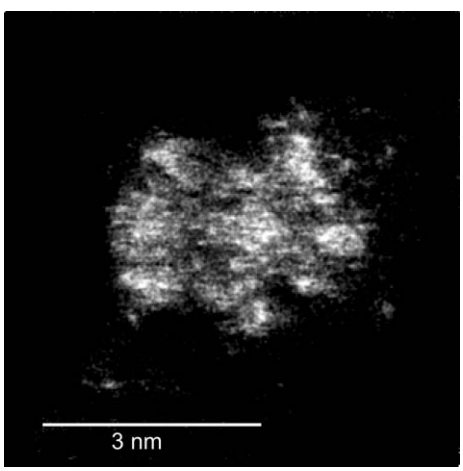

Fig. 3 STEM HAADF image of a loose agglomerate of $Ru_{10}Pt_2$ clusters.

Various kinds of high-level computations have been carried out[11–13] on metallic clusters, the majority being concerned with the structures of the clusters in free space or in the condensed state. Considerable attention has also been paid to clusters of gold (and of palladium) anchored to F-centres at MgO surfaces.[14] In a combined EXAFS–molecular mechanics and *ab initio* study[15] of $Ru_{12}Cu_4C_2$ bound to the oxygen atoms of the silica, a satisfactory picture emerged of the internal structure of the anchored nanoparticle, in line with the notion that such bimetallic entities are best pictured as strongly adsorbed molecules. For clusters of gold atoms, Cleveland *et al.*[13] have used atomistic models to identify three regimes in the size evolution of gold. A transition from molecular to ordered non-crystallographic structures occurred when the number of atoms approached 40. A further transition to crystallinity and bulk lattice structure was predicted at around 250 atoms. In the present work on $Ru_{10}Pt_2$ we find a threshold at around 200 atoms. For volumes substantially below this, crystallinity is not detected. For some nanoparticles approaching a size of 200 atoms, the onset of ordering is apparent, while for many of the larger nanoparticles, clear crystalline character is observed (see Fig. 4).

It would be prudent to carry out further work on two fronts. First, a combination of the use of aberration corrected microscopy and dark field STEM tomography,[16] in order to learn more about the internal structure and external facetting of the larger bimetallic nanoparticles. Second, to trace the changes in electronic properties, and parallel changes in catalytic performance, that accompany the

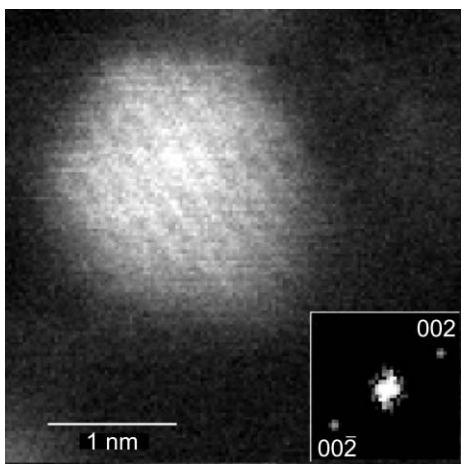

Fig. 4 Crystalline nanoparticle, formed *via* the coalescence of $Ru_{10}Pt_2$ precursors prior to catalysis. The crystal lattice fringes, clearly resolved as shown in the inset Fourier transform (calculated diffraction pattern), correspond to a spacing of 2.1 $\pm$ 0.2 Å, compared to the (002) Ru spacing of 2.14 Å. Facets of the crystal can also be observed.

transition from the molecular to the crystalline states of the bimetallic nanoparticles.

We are grateful to the the EPSRC for financial support (to EPWW) and for a grant (to PAM and JMT), and to the Royal Society and the National Science Foundation (for IA).

Notes and references

† The preparation of $Ru_{10}Pt_2$ nanoparticles from their parent carbonylate, and verification of their composition, has been described previously.[1,2,6,8] The silica used was of the MCM-41 type,[17] prepared as hitherto described.[2]

‡ Software scripts, written in IDL,[10] were used to quantify the nanoparticle distribution from STEM HAADF images. A semi-automatic data collection strategy involved manual identification of particles, integrated with automatic calculation of particle projected areas and their total intensities. The Laplacian of Gaussian (LoG) filter was found to be effective in accurately detecting particles against the modulated, rather noisy background present in STEM images of interest, such as in Fig. 2. The LoG filter, which was applied as a single discrete 9 × 9 kernel in image space involves the convolution of the edge-finding Laplacian with a Gaussian smoothing operator.[18] The kernel values were calculated for a Gaussian standard deviation, σ, of 1.4, with matrix values given by:

$$LoG(x, y) = -\frac{1}{\pi\sigma^4}\left[1 - \frac{x^2 + y^2}{2\sigma^2}\right]\exp\left(-\frac{x^2 + y^2}{2\sigma^2}\right).$$

1 J. M. Thomas, B. F. G. Johnson, R. Raja, G. Sankar and P. A. Midgley, *Acc. Chem. Res.*, 2003, **36**, 20.
2 J. M. Thomas and R. Raja, *J. Organomet. Chem.*, 2004, **689**, 4110.
3 These four active catalysts, unlike others that are equally active such as Ru_6Pd_6 and Ru_6Sn, also contain interstitial atoms of carbon: to be precise the four cited examples are more properly designated $Ru_{12}Cu_4C_2$, $Ru_{12}Ag_4C_2$, Ru_5PtC and $Ru_{10}Pt_2C_2$.
4 D. S. Shephard, T. Maschmeyer, B. F. G. Johnson, J. M. Thomas, G. Sankar, D. Ozkaya, W. Z. Zhou, R. D. Oldroyd and R. G. Bell, *Angew. Chem., Int. Ed.*, 1997, **36**, 2242.
5 W. Z. Zhou, J. M. Thomas, D. S. Shephard, B. F. G. Johnson, D. Ozkaya, T. Maschmeyer, R. G. Bell and Q. F. Ge, *Science*, 1998, **280**, 705.
6 P. A. Midgley, J. M. Thomas, L. Laffont, M. Weyland, R. Raja, B. F. G. Johnson and T. Khimyak, *J. Phys. Chem. B*, 2004, **108**, 4590.
7 U. Falke, A. L. Bleloch, M. Falke and A. Kolodzie, *Inst. Phys. Conf. Ser.*, 2003, **180**, 533.
8 J. M. Thomas, R. Raja, B. F. G. Johnson, T. J. O'Connell, G. Sankar and T. Khimyak, *Chem. Commun.*, 2003, 1126; see also *Science*, 2003, **300**, 867.
9 P. A. Midgley, M. Weyland, J. M. Thomas and B. F. G. Johnson, *Chem. Commun.*, 2001, 907.
10 Research Systems Incorporated, 2005, Interactive Data Language version 6.1.
11 K. Albert, K. M. Neyman, G. Pacchioni and N. Rösch, *Inorg. Chem.*, 1996, **35**, 7370.
12 A. V. Matveev, K. M. Neyman, G. Pacchioni and N. Rösch, *Chem. Phys. Lett.*, 1999, **299**, 603.
13 C. L. Cleveland, U. Landman, T. G. Schaaff, M. N. Shafigullin, P. W. Stephens and R. L. Whetten, *Phys. Rev. Lett.*, 1997, **79**, 1873.
14 B. Yoon, H. Hakkinen, U. Landman, A. S. Worz, J. M. Antonietti, S. Abbet, K. Judai and U. Heiz, *Science*, 2005, **307**, 403.
15 S. T. Bromley, G. Sankar, C. R. A. Catlow, T. Maschmeyer, B. F. G. Johnson and J. M. Thomas, *Chem. Phys. Lett.*, 2001, **340**, 524.
16 J. M. Thomas, P. A. Midgley, T. J. V. Yates, J. S. Barnard, R. Raja, I. Arlsan and M. Weyland, *Angew. Chem., Int. Ed.*, 2004, **43**, 6745.
17 C. T. Kresge, M. E. Leonowicz, W. J. Roth, J. C. Vartuli and J. S. Beck, *Nature*, 1992, **359**, 710.
18 M. Demi, *Comput. Vis. Image Und.*, 2005, **97**, 180.